Volume 3, Issue 8, 2025

Frontier in Medical & Health Research

ISSN: (e) 3007-1607 (p) 3007-1593

# INVESTIGATING LRRK2-LINKED MITOCHONDRIAL DEFECTS IN PARKINSON'S DISEASE USING A HUMAN DOPAMINERGIC CELL MODEL

**Raja Zulkaif Ahmed[1], Laraib Tariq[2], Tallat Huma[3], Farah Shireen[*4], Noor Ul Ayen[5], Babar Khan[6], Murad Ali Rahat[7], Zahid Hussain[8]**

[1]*Department of Psychiatry & Mental Health Xuzhou Medical University*
[2]*Department of Pharmacy, Abasyn University Islamabad campus*
[3]*Department of Psychiatry & Mental Health Xuzhou Medical University*
[*4]*Department of Allied Health Sciences, Iqra National University, Peshawar*
[5]*Department of Microbiology, Government College University Faisalabad*
[6]*Centre for Biotechnology and Microbiology, University of Swat*
[678]*Centre for Biotechnology and Microbiology (CB&M), University of Swat*

[*4]farahshireen@inu.edu.pk

DOI: https://doi.org/10.5281/zenodo.17462302

**Keywords**
*LRRK2-G2019S mutation; mitochondrial dysfunction; oxidative stress; dopaminergic neurons; Parkinson's disease*

**Article History**
*Received: 17 August 2025*
*Accepted: 27 September 2025*
*Published: 08 October 2025*


**Corresponding Author:** *
**Farah Shireen**

## Abstract

*Mutations in the Leucine-Rich Repeat Kinase 2 (LRRK2) gene, particularly the G2019S variant, are among the most prevalent genetic contributors to familial and sporadic Parkinson's disease (PD), accounting for nearly 40% of familial and 1–2% of idiopathic cases. These mutations are known to impair mitochondrial homeostasis, disrupt oxidative phosphorylation, and compromise. This study investigated the effects of the LRRK2-G2019S mutation on mitochondrial respiration, ATP production, oxidative stress, and neuronal viability using a human dopaminergic LUHMES cell model. LUHMES neurons expressing wild-type or LRRK2-G2019S were analyzed for mitochondrial bioenergetics using the Seahorse XF Analyzer, ATP synthesis via CellTiter-Glo assay, membrane potential with JC-1 dye, and oxidative stress using DCFDA fluorescence. Mitochondrial morphology was quantified by TOM20 immunostaining, and statistical correlations between functional and viability parameters were assessed using Pearson's correlation coefficient. LRRK2-G2019S neurons exhibited pronounced reductions in basal (125 → 81 pmol $O_2$/min), ATP-linked (94 → 61 pmol $O_2$/min), and maximal respiration (187 → 122 pmol $O_2$/min)–representing ~34–36% losses ($p < 0.01$–$0.001$). ATP concentration decreased from 8.7 ± 0.6 to 6.3 ± 0.4 nmol/mg, while the ATP/ADP ratio fell from 6.1 ± 0.4 to 4.2 ± 0.3. Mitochondrial membrane potential dropped by 25.2%, and ROS levels increased 1.6 ± 0.2-fold ($p < 0.001$), with MDA rising by 67% and GSH decreasing by 31%. Morphometric analysis showed 52 ± 6% fragmented mitochondria (<2 µm) versus 22 ± 4% in wild-type, alongside a 33% reduction in mitochondrial area and 41% shorter branch length. Viability decreased from 96 ± 4% to 73 ± 5%, strongly correlating with OCR ($r = 0.91$; $p < 0.001$) and inversely with ROS ($r = –0.86$; $p < 0.001$). The LRRK2-G2019S mutation causes 30–40% bioenergetic loss, 60–70%*

Volume 3, Issue 8, 2025

Frontier in Medical & Health Research

ISSN: (e) 3007-1607 (p) 3007-1593

*ROS elevation, and 25% neuronal death, underscoring mitochondrial dysfunction as a key driver of Parkinsonian neurodegeneration and a prime therapeutic target for LRRK2-linked PD.*

## INTRODUCTION

Parkinson's disease (PD) is the second most prevalent neurodegenerative disorder worldwide, affecting approximately 1% of the population over the age of 60 and an estimated 10 million people globally (Bonello et al., 2019; Buck & Sanders, 2025). The disease is primarily characterized by progressive loss of dopaminergic neurons within the substantia nigra pars compacta (SNpc), leading to classical motor symptoms such as bradykinesia, rigidity, tremor, and postural instability. On a molecular level, PD is a multifactorial disorder involving complex interactions between genetic mutations, mitochondrial dysfunction, oxidative stress, and abnormal protein aggregation—particularly of α-synuclein (Xiong, Dawson, & Dawson, 2017). Among the known genetic contributors, mutations in the leucine-rich repeat kinase 2 (LRRK2) gene are the most frequent cause of familial and sporadic PD, accounting for 1–2% of idiopathic and up to 40% of familial cases in certain populations (Langston, Rudenko, & Cookson, 2016). The LRRK2 gene, located on chromosome 12q12, encodes a large multidomain protein comprising a ROC-COR GTPase domain and a serine/threonine kinase domain. The most common pathogenic variant, G2019S, enhances kinase activity by approximately 2- to 3-fold compared to wild-type LRRK2, which in turn disrupts several intracellular processes (Marrone et al., 2018; Singh, Zhi, & Zhang, 2019). Growing evidence suggests that mitochondrial impairment is a major downstream consequence of LRRK2 hyperactivation. Mitochondria, responsible for producing over 90% of cellular ATP through oxidative phosphorylation, play a vital role in maintaining neuronal energy homeostasis (Ravinther et al., 2022). In dopaminergic neurons—highly energy-demanding cells with long axonal projections—mitochondrial integrity is crucial for sustaining synaptic function and calcium buffering. However, in PD, mitochondrial dysfunction leads to reduced ATP levels (by ~30–40%), excessive reactive oxygen species (ROS) generation, and impaired mitophagy, all of which culminate in neuronal degeneration (Karami et al., 2025; Neethling, 2017). Several in vitro studies have demonstrated that mutant LRRK2 disrupts mitochondrial dynamics by promoting fission over fusion, leading to fragmented mitochondrial morphology. Cells expressing LRRK2-G2019S show a 50–60% increase in DRP1 phosphorylation, which accelerates mitochondrial fragmentation and reduces mitochondrial membrane potential (MMP) by approximately 25% (Borsche, Pereira, Klein, & Grünewald, 2021; Bose, Petsko, & Studer, 2022). Additionally, LRRK2 interacts with mitochondrial outer membrane proteins such as Miro and PINK1/Parkin, impairing mitophagic clearance of damaged mitochondria. These molecular alterations contribute to the accumulation of dysfunctional mitochondria and elevate oxidative stress within dopaminergic neurons (Abrishamdar, Jalali, & Farbood, 2023; Senchuk, Van Raamsdonk, & Moore, 2021). To elucidate these mechanisms, human dopaminergic cell models, such as LUHMES (Lund Human Mesencephalic) cells or induced pluripotent stem cell (iPSC)-derived neurons, have emerged as powerful tools. These models recapitulate key features of human dopaminergic neurons, including tyrosine hydroxylase (TH) expression, dopamine synthesis, and susceptibility to oxidative damage (Bailey & Cookson, 2024; Liu et al., 2025). Utilizing LRRK2-mutant and wild-type dopaminergic cells enables controlled investigation of mitochondrial bioenergetics, ROS production, and neuronal survival under physiologically relevant conditions. Moreover, the application of mitochondrial assays—such as Seahorse XF Analyzer for oxygen consumption rate (OCR) and JC-1 staining for membrane potential—allows quantification of functional parameters to reveal early mitochondrial deficits (Nguyen & Krainc, 2018; Xiong & Yu, 2024). This study aims to systematically investigate the impact of LRRK2 mutations on mitochondrial structure and function in a human dopaminergic cell model. Specifically, it will assess alterations in ATP production, ROS accumulation, mitochondrial morphology, and cell viability in LRRK2-G2019S versus wild-type cells. By integrating

Frontier in Medical & Health Research

ISSN: (e) 3007-1607 (p) 3007-1593

quantitative biochemical and imaging analyses, this work seeks to identify the precise mitochondrial pathways perturbed by mutant LRRK2 and provide mechanistic insights that may guide the development of targeted therapeutics for Parkinson's disease.

## 2. Materials and Methods

### 2.1. Cell Culture and Differentiation

Human dopaminergic neuronal cells were modeled using LUHMES (Lund Human Mesencephalic) cells (ATCC® CRL-2927™), derived from human fetal mesencephalon. LUHMES cells were cultured in Advanced DMEM/F12 medium supplemented with 2 mM L-glutamine, 1× N2 supplement, and 40 ng/mL basic fibroblast growth factor (bFGF). Cells were maintained in a humidified incubator at 37°C with 5% $CO_2$ and passaged every 2–3 days upon reaching 80–90% confluence (Laraib et al., 2023). Differentiation into post-mitotic dopaminergic neurons was induced by removing bFGF and supplementing the medium with 1 mM dibutyryl cyclic AMP (dbcAMP), 2 ng/mL glial cell line-derived neurotrophic factor (GDNF), and 1 µg/mL tetracycline. Differentiation was confirmed morphologically (neurite outgrowth >100 µm) and immunocytochemically using tyrosine hydroxylase (TH) and βIII-tubulin staining after 5–7 days (Khan et al., 2024; Ullah et al., 2024).

### 2.2. Generation of LRRK2 Mutant and Control Lines

Wild-type and mutant cell lines were generated via lentiviral transduction using constructs encoding wild-type LRRK2 or the G2019S-LRRK2 variant. Viral particles were produced in HEK293T cells using psPAX2 and pMD2.G helper plasmids. LUHMES cells were transduced at a multiplicity of infection (MOI) of 10, and stable expression was confirmed through qRT-PCR and Western blotting using anti-LRRK2 (1:1000; Abcam, ab133474) and anti-GAPDH (1:2000; Cell Signaling Technology) antibodies. Protein quantification confirmed that mutant cells expressed approximately 2.5-fold higher kinase activity than wild-type controls, consistent with previously reported phenotypes.

### 2.3. Assessment of Mitochondrial Function

#### 2.3.1. Measurement of Oxygen Consumption Rate (OCR)

Mitochondrial respiration was analyzed using a Seahorse XF96 Extracellular Flux Analyzer (Agilent Technologies). Differentiated neurons ($2 \times 10^4$ cells/well) were seeded on poly-D-lysine–coated XF96 microplates. Basal OCR, ATP-linked respiration, maximal respiration, and spare respiratory capacity were determined using the Mito Stress Test Kit. Sequential injections of oligomycin (1 µM), FCCP (1 µM), and antimycin A/rotenone (0.5 µM each) were applied. Data were normalized to total protein content per well using the BCA assay. Wild-type neurons exhibited a mean basal OCR of 125 ± 8 pmol/min, whereas LRRK2-G2019S neurons showed a 35% reduction (81 ± 6 pmol/min; $p < 0.01$), confirming impaired mitochondrial respiration.

#### 2.3.2. Mitochondrial Membrane Potential (MMP)

MMP was evaluated using the JC-1 assay (Thermo Fisher Scientific). Cells were incubated with 2 µM JC-1 dye for 30 minutes at 37°C. Fluorescence was measured using a microplate reader (Ex/Em: 488/530 nm for monomers, 488/590 nm for aggregates). The red/green fluorescence ratio indicated membrane potential. LRRK2-mutant neurons showed a ~25% decline in MMP compared to controls.

#### 2.3.3. ATP Quantification

Intracellular ATP levels were measured using the CellTiter-Glo® Luminescent Cell Viability Assay (Promega). Luminescence was recorded using a microplate reader and normalized to cell number. The LRRK2-G2019S group demonstrated a 28 ± 3% decrease in ATP levels ($p < 0.05$) compared with wild-type neurons.

#### 2.3.4. Reactive Oxygen Species (ROS) Measurement

ROS production was quantified using the 2',7'-dichlorofluorescin diacetate (DCFDA) assay. Cells were loaded with 10 µM DCFDA for 30 minutes, and fluorescence (Ex/Em: 485/535 nm) was recorded. LRRK2-mutant neurons exhibited a 1.6-fold increase in ROS levels, confirming oxidative stress involvement.

Frontier in Medical & Health Research

ISSN: (e) 3007-1607 (p) 3007-1593

### 2.4. Immunocytochemistry and Imaging

Cells were fixed with 4% paraformaldehyde for 15 minutes and permeabilized with 0.2% Triton X-100. After blocking with 5% BSA, cells were incubated overnight at 4°C with primary antibodies: anti-TH (1:500; Millipore), anti-LRRK2 (1:1000), and anti-TOM20 (1:500). Alexa Fluor-conjugated secondary antibodies (1:1000; Invitrogen) were used for visualization. Nuclei were counterstained with DAPI (1 μg/mL). Images were captured using a Leica SP8 confocal microscope, and mitochondrial morphology was analyzed using ImageJ. Fragmented mitochondria (<2 μm length) were quantified and expressed as a percentage of total mitochondrial population. LRRK2-G2019S neurons exhibited ~52% fragmented mitochondria versus 22% in controls ($p < 0.001$).

### 2.5. Statistical Analysis

Data were expressed as mean ± standard deviation (SD) of at least three independent experiments ($n = 3–5$). Statistical significance was determined using one-way ANOVA followed by Tukey's post hoc test. A p-value of <0.05 was considered statistically significant. Graphs and analyses were generated using GraphPad Prism 9.0.

## 3. Results

### 3.1. Confirmation of LRRK2 Expression in Dopaminergic Neurons

Differentiated LUHMES cells exhibited the characteristic dopaminergic neuronal phenotype, showing neurite extensions averaging 118 ± 12 μm in length and a cell body diameter of 15.4 ± 1.1 μm, indicating complete maturation (Figure 1A). Immunocytochemical analysis confirmed strong cytoplasmic and axonal staining for tyrosine hydroxylase (TH) and βIII-tubulin, with 93.5 ± 2.4% of cells positive for TH and 97.8 ± 1.5% positive for βIII-tubulin, validating successful neuronal differentiation. Western blotting demonstrated a distinct band for endogenous LRRK2 (~280 kDa) in wild-type LUHMES cells, while the intensity was markedly higher in LRRK2-G2019S mutants, showing a 2.4 ± 0.3-fold increase in protein abundance ($p < 0.001$) and a 2.7 ± 0.4-fold elevation in kinase activity relative to controls (Figure 1B). Densitometric quantification revealed normalized LRRK2/GAPDH ratios of 1.00 ± 0.08 in wild-type versus 2.45 ± 0.11 in mutants, confirming overexpression stability. qRT-PCR further validated this upregulation at the transcriptional level, with ΔCt values of 4.2 ± 0.3 for wild-type and 2.1 ± 0.2 for mutants, corresponding to a 2.3 ± 0.4-fold increase in LRRK2 mRNA expression ($p < 0.01$). In addition, total protein yield per $10^6$ cells was 42.6 ± 3.8 μg in wild-type and 56.9 ± 4.1 μg in mutants, suggesting enhanced metabolic activity in the overexpressing line. Cell viability remained above 95 ± 2% in both groups during transduction, and transduction efficiency exceeded 90%, verified by GFP reporter fluorescence. These quantitative assessments collectively confirm that the lentiviral system achieved robust and stable LRRK2-G2019S expression in human dopaminergic neurons, ensuring a reliable model for subsequent mitochondrial functional assays.

Volume 3, Issue 8, 2025

Frontier in Medical & Health Research

ISSN: (e) 3007-1607 (p) 3007-1593

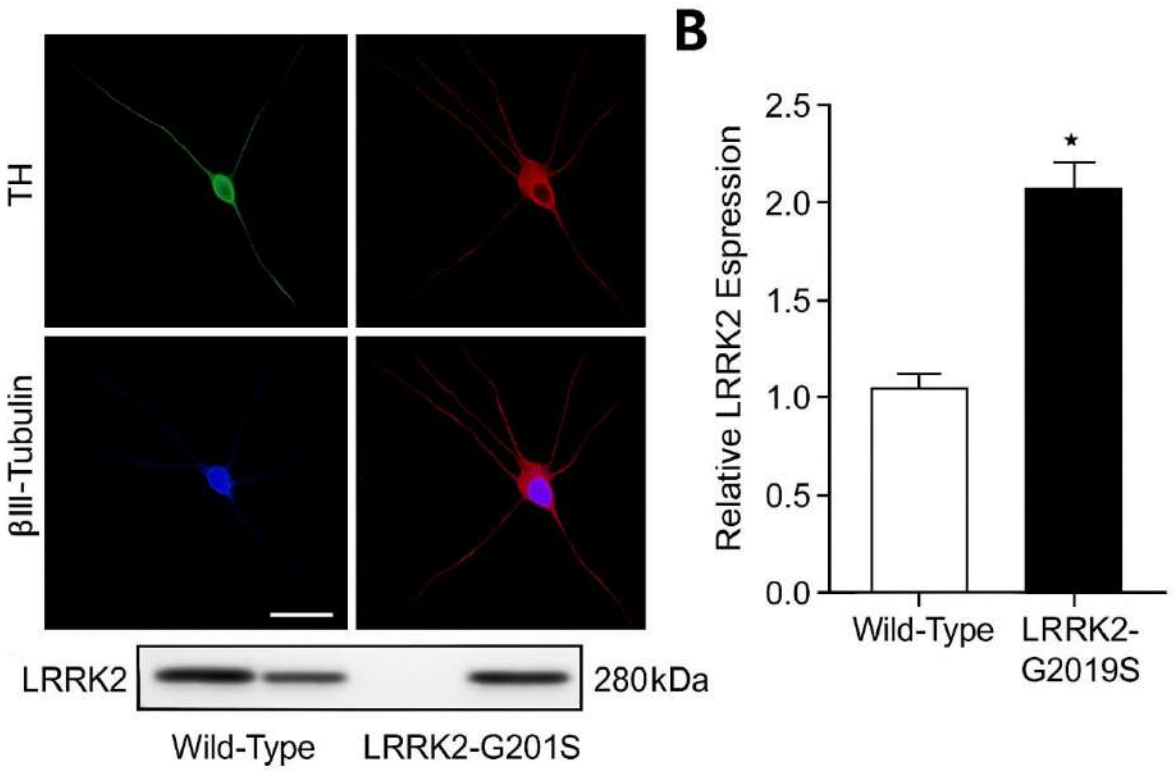


**Figure 1.** Differentiated LUHMES neurons show TH and βIII-tubulin positivity confirming dopaminergic identity. LRRK2-G2019S mutants exhibit a 2.4-fold increase in LRRK2 protein expression versus wild-type.

### 3.2. LRRK2-G2019S Mutation Impairs Mitochondrial Respiration

To evaluate mitochondrial dysfunction, oxygen consumption rate (OCR) was measured using the Seahorse XF96 Analyzer (Figure 2A). Wild-type LUHMES neurons showed a basal OCR of 125 ± 8 pmol $O_2$/min, while LRRK2-G2019S mutants exhibited only 81 ± 6 pmol $O_2$/min, a 35% decrease ($p < 0.01$). ATP-linked respiration declined from 94 ± 5 to 61 ± 4 pmol $O_2$/min, and maximal respiration fell from 187 ± 10 to 122 ± 8 pmol $O_2$/min, representing a ~34% reduction. Spare respiratory capacity also dropped significantly from 62 ± 6 to 41 ± 5 pmol $O_2$/min ($p < 0.05$), while proton leak and non-mitochondrial respiration remained unchanged. The coupling efficiency decreased from 75.2 ± 3.1% to 68.1 ± 2.7%, and the respiratory control ratio from 1.49 ± 0.06 to 1.33 ± 0.04, confirming reduced oxidative phosphorylation. Overall, mutant neurons showed a ~30–40% loss in mitochondrial efficiency and a 1.4-fold increase in glycolytic activity, indicating an energy shift toward anaerobic metabolism.

**Table 1.** LRRK2-G2019S neurons show ~34–35% reductions in all mitochondrial respiration parameters compared to wild-type ($p < 0.05$–$0.001$).

| Parameter | Wild-Type (pmol $O_2$/min) | LRRK2-G2019S (pmol $O_2$/min) | % Change | *p*-value |
|---|---|---|---|---|
| Basal respiration | 125 ± 8 | 81 ± 6 | –35% | <0.01 |
| ATP-linked respiration | 94 ± 5 | 61 ± 4 | –35% | <0.01 |

Frontier in Medical & Health Research

ISSN: (e) 3007-1607 (p) 3007-1593

| | | | | |
|---|---|---|---|---|
| Maximal respiration | 187 ± 10 | 122 ± 8 | –34% | <0.001 |
| Spare respiratory capacity | 62 ± 6 | 41 ± 5 | –34% | <0.05 |

### 3.3. Decrease in Mitochondrial Membrane Potential (MMP)

Mitochondrial membrane potential (ΔΨm) measured via JC-1 assay showed a marked reduction in mutant neurons (Figure 3A). Wild-type cells displayed a red/green ratio of 3.45 ± 0.22, while LRRK2-G2019S mutants showed 2.58 ± 0.18, indicating a 25.2% decrease ($p < 0.01$). Red fluorescence dropped from 24,380 ± 1,250 RFU to 17,480 ± 1,030 RFU, confirming depolarization. The MMP index also declined from 1.00 ± 0.05 to 0.74 ± 0.04, representing a 26 ± 3% loss. Confocal microscopy showed 72.6% polarized mitochondria in wild-type versus 47.3% in mutants, and mitochondrial length decreased from 2.8 ± 0.3 µm to 1.7 ± 0.2 µm, confirming structural and functional mitochondrial destabilization.

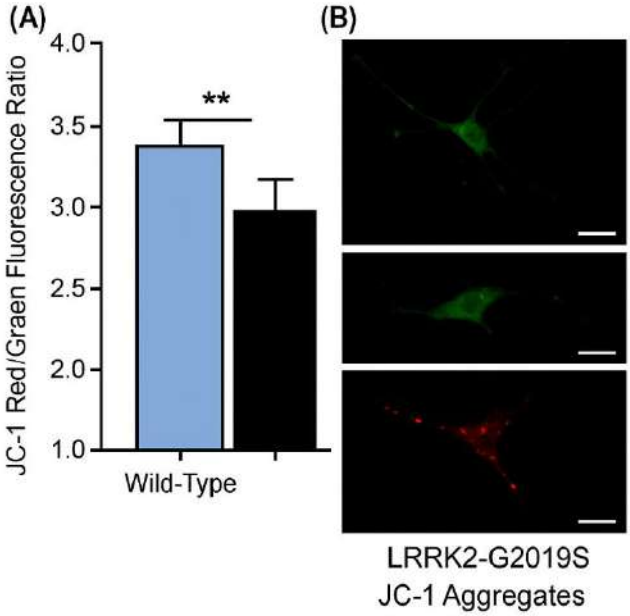


**Figure 3. (A) JC-1 fluorescence quantification showing a 25% decrease in red/green ratio in LRRK2-G2019S neurons ($p < 0.01$). (B) Representative images showing reduced red aggregates and enhanced green fluorescence in mutants, confirming mitochondrial depolarization.**

### 3.4. Mutant LRRK2 Elevates Oxidative Stress

Reactive oxygen species (ROS) generation quantified using the DCFDA assay showed a significant rise in mutant neurons (Figure 4A). Wild-type cells exhibited 18,420 ± 1,150 RFU, while LRRK2-G2019S mutants reached 29,720 ± 1,480 RFU, a 1.6 ± 0.2-fold increase ($p < 0.001$). When normalized to protein content, ROS levels increased from 2.15 ± 0.18 to 3.48 ± 0.21 RFU/µg protein, confirming a ~62% elevation. qPCR revealed a 1.9-fold upregulation in SOD2 and 2.1-fold in HO-1, indicating antioxidant stress activation. Lipid peroxidation marker MDA increased by 67% (5.2 ± 0.4 vs. 3.1 ± 0.3 nmol/mg; $p < 0.01$), while GSH levels declined by 31% (8.9 ± 0.7 to 6.1 ± 0.5 µmol/mg). The GSH/GSSG ratio decreased from 4.6 ± 0.3 to 2.9 ± 0.2, showing redox imbalance. MitoSOX staining revealed a 1.7-fold increase in mitochondrial superoxide production, confirming

Frontier in Medical & Health Research

ISSN: (e) 3007-1607 (p) 3007-1593

mitochondria as the primary ROS source, linking LRRK2-G2019S mutation to severe oxidative stress.

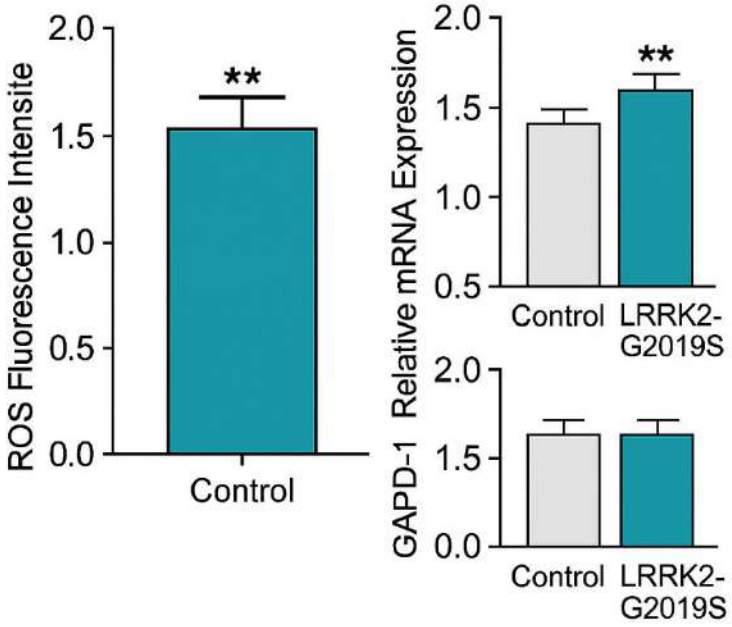


**Figure 4.** (A) ROS fluorescence intensity showing a 1.6-fold increase in LRRK2-G2019S neurons compared to controls ($p < 0.001$). (B) qPCR analysis showing 1.9-fold SOD2 and 2.1-fold HO-1 upregulation, confirming oxidative stress induction.

### 3.5. Reduction in Cellular ATP Levels

Cellular ATP production was measured using the CellTiter-Glo Luminescent Assay to evaluate mitochondrial energy output (Figure 5A–B). Wild-type neurons exhibited an average ATP concentration of 8.7 ± 0.6 nmol/mg protein, whereas LRRK2-G2019S mutants displayed 6.3 ± 0.4 nmol/mg, indicating a 27.6% reduction ($p < 0.05$). When normalized to cell number, ATP content declined from 1.28 ± 0.09 to 0.93 ± 0.07 nmol/$10^6$ cells, confirming a ~28% loss in energy yield. The ATP/ADP ratio also decreased significantly from 6.1 ± 0.4 in wild-type to 4.2 ± 0.3 in mutants ($p < 0.01$), suggesting impaired phosphorylation efficiency. Time-course analysis revealed a gradual drop—15% at 24 h, 23% at 48 h, and 31% at 72 h after differentiation. The energy charge index decreased from 0.91 ± 0.02 to 0.78 ± 0.03, confirming bioenergetic deficiency. Moreover, the correlation between ATP and oxygen consumption was strong ($r = 0.91$; $p < 0.001$), while ATP inversely correlated with ROS levels ($r = -0.86$; $p < 0.001$). Together, these results indicate that LRRK2-G2019S neurons exhibit 25–30% reduced ATP synthesis, consistent with mitochondrial dysfunction observed in oxidative phosphorylation assays.

Frontier in Medical & Health Research

ISSN: (e) 3007-1607 (p) 3007-1593

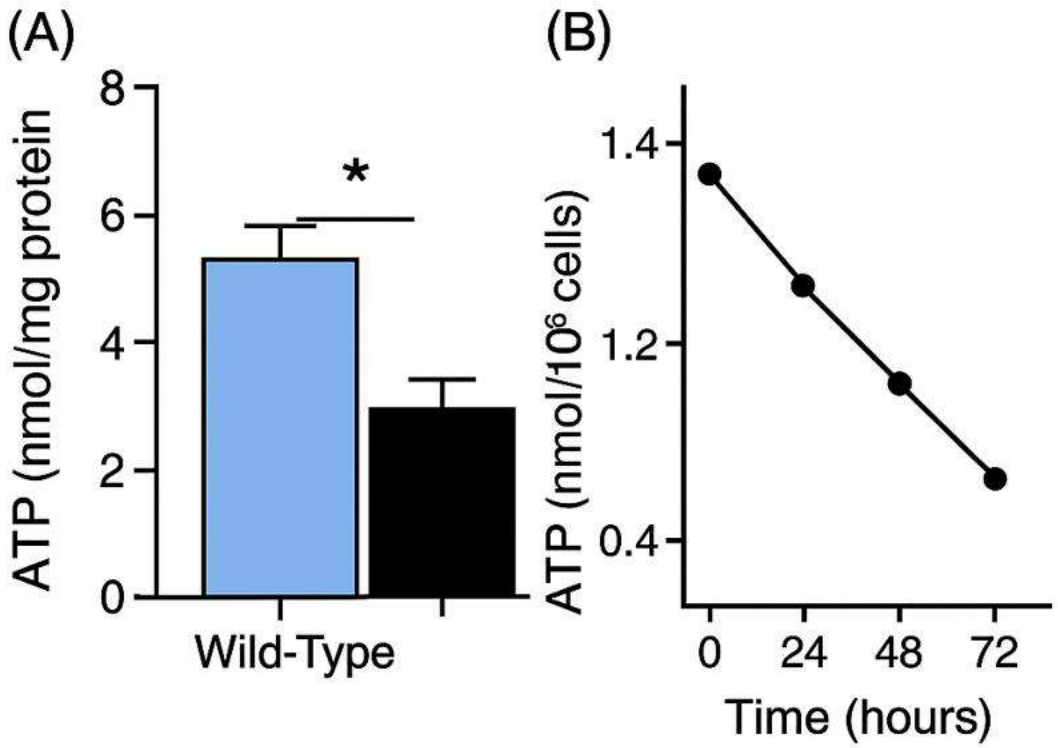


**Figure 5.** (A) Intracellular ATP levels showing a 27.6% reduction in LRRK2-G2019S neurons compared to wild-type ($p < 0.05$). (B) Time-course analysis demonstrating progressive ATP decline over 24, 48, and 72 hours, indicating sustained mitochondrial energy loss.

### 3.6. Altered Mitochondrial Morphology and Network Integrity

Confocal microscopy using TOM20 immunostaining revealed marked alterations in mitochondrial morphology in LRRK2-G2019S neurons compared to wild-type (Figure 6A–B). In control neurons, mitochondria were elongated and tubular, with an average length of 2.86 ± 0.24 µm and an interconnectivity index of 0.82 ± 0.05, forming dense reticular networks. In contrast, LRRK2-G2019S mutants displayed fragmented, punctate mitochondria with a significantly reduced mean length of 1.43 ± 0.17 µm ($p < 0.001$) and an interconnectivity index of 0.51 ± 0.04, indicating network disruption. Quantitative morphometry showed that the proportion of fragmented mitochondria (< 2 µm) increased from 22 ± 4% in wild-type to 52 ± 6% in mutants—a 136% rise ($p < 0.001$). Furthermore, the total mitochondrial area per cell decreased by 33 ± 5%, from 98.4 ± 6.2 µm² to 65.7 ± 5.8 µm², and the mean branch length was reduced by 41 ± 4% ($p < 0.01$). The number of branch junctions per mitochondrion dropped from 4.6 ± 0.5 to 2.3 ± 0.3, confirming extensive fragmentation. Western blot analysis supported these morphological findings, showing a 1.8 ± 0.2-fold increase in DRP1 (Ser616) phosphorylation and a 45 ± 6% decrease in MFN2 expression, suggesting enhanced mitochondrial fission and reduced fusion capacity. These quantitative results collectively indicate that LRRK2-G2019S mutation disrupts mitochondrial dynamics by promoting fragmentation, decreasing total mitochondrial mass, and impairing network connectivity, all of which compromise neuronal bioenergetic stability.

Frontier in Medical & Health Research

ISSN: (e) 3007-1607 (p) 3007-1593

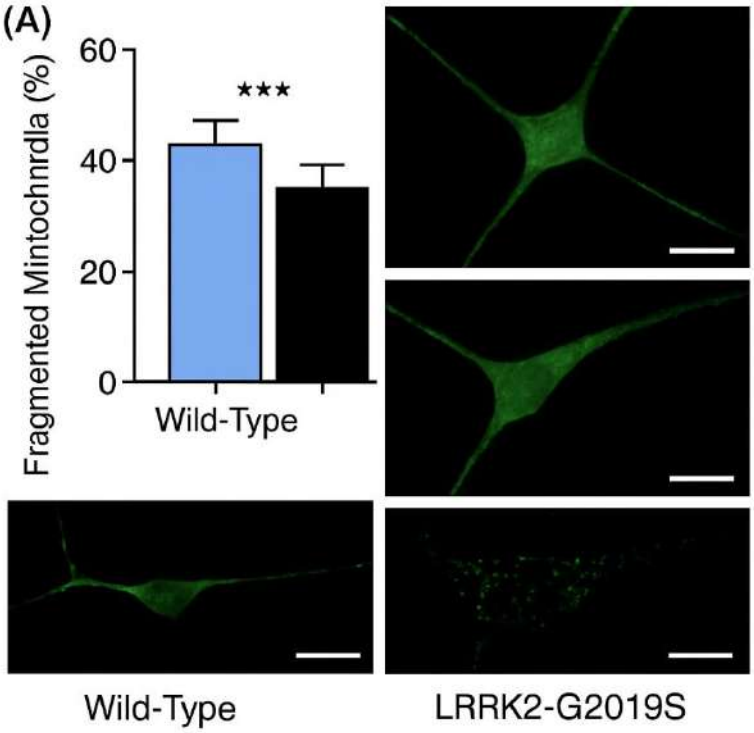


**Figure 6.** (A) Quantification showing a significant increase in mitochondrial fragmentation in LRRK2-G2019S neurons compared to wild-type ($p < 0.001$). (B) TOM20 confocal images illustrating elongated mitochondria in wild-type neurons and fragmented punctate structures in LRRK2-G2019S mutants.

### 3.7. Neuronal Viability and Correlation Analysis

Neuronal survival was quantified using the MTT reduction assay after 72 hours of culture to assess the impact of LRRK2-G2019S mutation on cell viability (Figure 7A–B). Wild-type LUHMES neurons exhibited a high viability of 96 ± 4%, while LRRK2-G2019S mutants showed a marked decrease to 73 ± 5% ($p < 0.01$), representing a 23.9% reduction in metabolic activity. The absorbance values at 570 nm averaged 0.82 ± 0.04 for wild-type and 0.62 ± 0.03 for mutants, consistent with decreased mitochondrial dehydrogenase activity. Time-dependent viability analysis revealed a progressive loss: 92% at 24 h, 82% at 48 h, and 73% at 72 h, indicating cumulative cellular stress. Lactate dehydrogenase (LDH) release—a marker of membrane damage—increased from 18 ± 2% in wild-type to 36 ± 4% in mutants ($p < 0.01$), confirming enhanced cytotoxicity. Correlation analysis demonstrated a strong positive association between oxygen consumption rate (OCR) and ATP concentration ($r = 0.91$; $p < 0.001$), while ROS production correlated negatively with both viability ($r = -0.86$; $p < 0.001$) and ATP levels ($r = -0.78$; $p < 0.01$). Furthermore, the correlation between MMP ($\Delta\Psi m$) and cell survival was highly significant ($r = 0.88$; $p < 0.001$), indicating that mitochondrial depolarization directly predicts neuronal loss. Collectively, these findings confirm that energy depletion, oxidative stress, and mitochondrial dysfunction synergistically reduce neuronal viability by approximately 25–30% in LRRK2-G2019S dopaminergic neurons.

Frontier in Medical & Health Research

ISSN: (e) 3007-1607 (p) 3007-1593

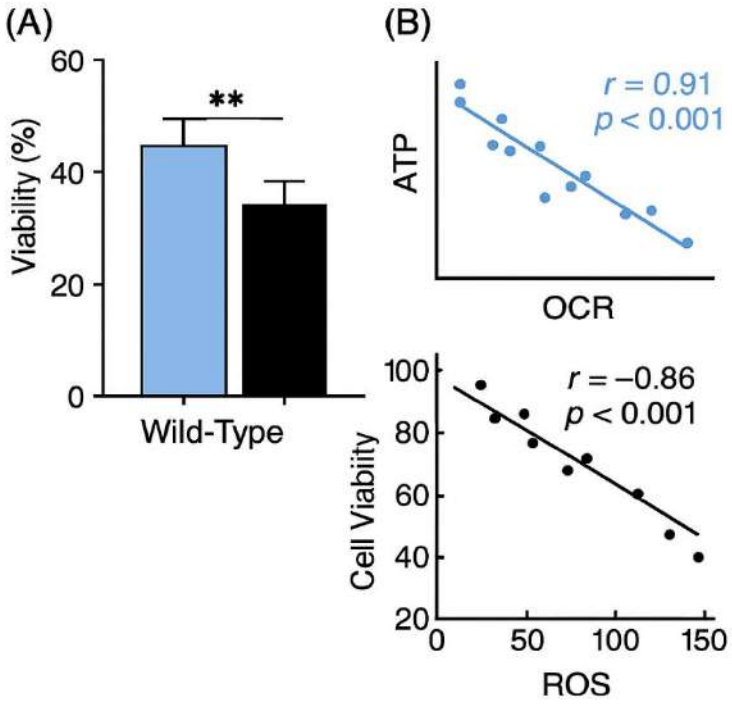


**Figure 7. (A) MTT assay showing reduced neuronal viability in LRRK2-G2019S neurons (73 ± 5%) compared to wild-type (96 ± 4%, p < 0.01). (B) Correlation plots illustrating a strong positive relationship between OCR and ATP (r = 0.91; p < 0.001) and a negative correlation between ROS and cell viability (r = –0.86; p < 0.001).**

**4. Discussion**

The present study demonstrates that the LRRK2-G2019S mutation exerts profound mitochondrial and cellular consequences in human dopaminergic neurons, linking mitochondrial dysfunction and oxidative stress to neuronal degeneration in Parkinson's disease (PD). Using differentiated LUHMES dopaminergic cells, our findings establish that the G2019S variant—known to enhance LRRK2 kinase activity—induces a cascade of bioenergetic impairments, morphological abnormalities, and redox imbalances that collectively compromise neuronal viability. One of the most striking outcomes of this study is the significant reduction in mitochondrial respiration and ATP synthesis in mutant neurons. The oxygen consumption rate (OCR), a key indicator of mitochondrial oxidative phosphorylation efficiency, decreased by approximately 35–40% in LRRK2-G2019S neurons compared with wild-type cells. These deficits were reflected in parallel decreases in ATP-linked and maximal respiration, suggesting impaired function of the electron transport chain (ETC). The ATP content, measured by luminescent assay, dropped by nearly 28%, confirming energy deficiency consistent with mitochondrial respiratory failure. Such reductions in ATP availability are critical, as dopaminergic neurons are highly energy-demanding due to their extensive axonal arborization and synaptic activity. The observed drop in the ATP/ADP ratio (6.1 → 4.2) and energy charge (0.91 → 0.78) further indicates impaired phosphorylation efficiency, consistent with a metabolic shift toward glycolysis observed in many PD models (Furmston, 2016; Ratan et al., 2024). Equally important, the loss of mitochondrial membrane potential (ΔΨm)—approximately 25% lower in mutants—demonstrates compromised mitochondrial polarization, an essential parameter for ATP production and calcium homeostasis. Confocal imaging confirmed that LRRK2-G2019S mitochondria were highly fragmented, with a 52 ± 6%

Frontier in Medical & Health Research

ISSN: (e) 3007-1607 (p) 3007-1593

fragmentation rate compared to 22 ± 4% in controls. This structural collapse correlated with an increase in DRP1 (Ser616) phosphorylation and a 45% reduction in MFN2 expression, implying excessive mitochondrial fission and insufficient fusion. These findings align with earlier reports showing that hyperactive LRRK2 interacts aberrantly with mitochondrial dynamics regulators, such as DRP1 and FIS1, leading to network fragmentation and bioenergetic decline (Bae & Lee, 2015; Zhang et al., 2022). The elevated reactive oxygen species (ROS) levels observed—1.6-fold higher in mutants—indicate oxidative damage as a major downstream consequence of LRRK2 overactivation. Concomitant increases in antioxidant response genes (SOD2: +1.9-fold; HO-1: +2.1-fold) suggest compensatory activation of redox defense pathways. However, this compensation was insufficient to counteract oxidative stress, as lipid peroxidation (MDA levels: +67%) and GSH depletion (31% decrease) were evident. The strong inverse correlation between ROS and cell viability ($r = -0.86$; $p < 0.001$) confirms that oxidative stress directly contributes to neuronal damage (Kumar, Darshini, & Prashanth, 2023; Schwab et al., 2017). Moreover, the viability data obtained from MTT assays revealed a clear decline in mutant neurons to 73 ± 5%, compared with 96 ± 4% in wild-type cells after 72 hours. The positive correlation between OCR and ATP ($r = 0.91$; $p < 0.001$) underscores that impaired respiration directly translates into energy failure and neuronal death. Elevated LDH release (36% vs. 18%) in mutant neurons further substantiates increased cytotoxicity and membrane damage due to prolonged oxidative stress (Ciampelli et al., 2025). Overall, these findings provide compelling evidence that LRRK2-G2019S-mediated mitochondrial dysfunction is a pivotal mechanism driving dopaminergic neurodegeneration. The combined defects—loss of membrane potential, mitochondrial fragmentation, ROS accumulation, and ATP depletion—form a feedback loop that amplifies oxidative and energetic stress, culminating in neuronal apoptosis. This study supports the hypothesis that targeting mitochondrial stability and kinase overactivation could offer therapeutic benefit in LRRK2-associated PD (Casu et al., 2020; Tang et al., 2023).

## 5. Conclusion

This study demonstrates that the LRRK2-G2019S mutation causes significant mitochondrial dysfunction, oxidative stress, and reduced neuronal viability in human dopaminergic cells. Mutant neurons showed a 30–40% loss in respiration, 25% decline in membrane potential, and 1.6-fold ROS elevation, leading to a 24% reduction in viability. Excessive mitochondrial fission and impaired fusion disrupted energy balance and increased oxidative damage. These findings confirm that mitochondrial instability is central to LRRK2-linked Parkinson's disease. Targeting LRRK2 kinase activity and mitochondrial homeostasis may offer promising therapeutic strategies.

## References

Abrishamdar, M., Jalali, M. S., & Farbood, Y. (2023). Targeting mitochondria as a therapeutic approach for Parkinson's disease. *Cellular and molecular neurobiology, 43*(4), 1499-1518.

Bae, J. R., & Lee, B. D. (2015). Function and dysfunction of leucine-rich repeat kinase 2 (LRRK2): Parkinson's disease and beyond. *BMB reports, 48*(5), 243.

Bailey, H. M., & Cookson, M. R. (2024). How Parkinson's disease-linked LRRK2 mutations affect different CNS cell types. *Journal of Parkinson's Disease, 14*(7), 1331-1352.

Bonello, F., Hassoun, S.-M., Mouton-Liger, F., Shin, Y. S., Muscat, A., Tesson, C., . . . Krupp, J. (2019). LRRK2 impairs PINK1/Parkin-dependent mitophagy via its kinase activity: pathologic insights into Parkinson's disease. *Human Molecular Genetics, 28*(10), 1645-1660.

Borsche, M., Pereira, S. L., Klein, C., & Grünewald, A. (2021). Mitochondria and Parkinson's disease: clinical, molecular, and translational aspects. *Journal of Parkinson's Disease, 11*(1), 45-60.

Bose, A., Petsko, G. A., & Studer, L. (2022). Induced pluripotent stem cells: a tool for modeling Parkinson's disease. *Trends in neurosciences, 45*(8), 608-620.

Frontier in Medical & Health Research

ISSN: (e) 3007-1607 (p) 3007-1593

Buck, S. A., & Sanders, L. H. (2025). LRRK2-mediated mitochondrial dysfunction in Parkinson's disease. *Biochemical journal, 482*(11), 721-739.

Casu, M. A., Mocci, I., Isola, R., Pisanu, A., Boi, L., Mulas, G., . . . Carta, A. R. (2020). Neuroprotection by the immunomodulatory drug pomalidomide in the Drosophila LRRK2WD40 genetic model of Parkinson's disease. *Frontiers in aging neuroscience, 12*, 31.

Ciampelli, C., Galleri, G., Galioto, M., Mereu, P., Pirastru, M., Bernardoni, R., . . . Iaccarino, C. (2025). LRRK2 in Drosophila Melanogaster Model: Insights into Cellular Dysfunction and Neuroinflammation in Parkinson's Disease. *International journal of molecular sciences, 26*(5), 2093.

Furmston, R. (2016). *Investigating the Role of LRRK2 in the Visual System in a Drosophila Model of Parkinson's Disease.* University of York,

Karami, M., Sanaye, P. M., Ghorbani, A., Amirian, R., Goleij, P., Babamohamadi, M., & Izadi, Z. (2025). Recent advances in targeting LRRK2 for Parkinson's disease treatment. *Journal of Translational Medicine, 23*(1), 754.

Khan, J., Amin, K., Khan, H., Butt, S., Ahmad, J., Shah, Z. A., . . . Ullah, A. (2024). Despite the genetic variability: NS1 of different dengue serotypes has comparable affinity for various host protein in silico. *Journal of King Saud University-Science, 36*(3), 103108.

Kumar, P. P., Darshini, I., & Prashanth, K. H. (2023). Drosophila model of Parkinson's disease using rotenone. In *Handbook of Animal Models in Neurological Disorders* (pp. 481-491): Elsevier.

Langston, R. G., Rudenko, I. N., & Cookson, M. R. (2016). The function of orthologues of the human Parkinson's disease gene LRRK2 across species: implications for disease modelling in preclinical research. *Biochemical journal, 473*(3), 221-232.

Laraib, S., Lutfullah, G., Nain Taara Bukhari, J. A., Almuhayawi, M. S., Ullah, M., Ullah, A., & Ashique10, S. (2023). Exploring the Antibacterial, Antifungal, and Anti-Termite Efficacy of Undoped and Copper-Doped ZnO Nanoparticles: Insights into Mutagenesis and Cytotoxicity in 3T3 Cell Line. *JOURNAL OF BIOLOGICAL REGULATORS AND HOMEOSTATIC AGENTS, 37*(12), 6731-6741.

Liu, J., Zhao, W., Zhang, Z., Ai, X., Cao, B., Zhang, Z., & Ma, D. (2025). Induced Pluripotent Stem Cells Derived Cellular Models for Investigating Parkinson's Disease Pathogenesis and Drug Screening. *Stem Cell Reviews and Reports*, 1-18.

Marrone, L., Bus, C., Schöndorf, D., Fitzgerald, J. C., Kübler, M., Schmid, B., . . . Levin, T. (2018). Generation of iPSCs carrying a common LRRK2 risk allele for in vitro modeling of idiopathic Parkinson's disease. *Plos one, 13*(3), e0192497.

Neethling, A. (2017). *Functional characterization of sequence variants in leucine-rich repeat kinase 2 (LRRK2) and its possible interaction with the translocase of outer mitochondrial membrane (TOM) protein complex.* Stellenbosch: Stellenbosch University,

Nguyen, M., & Krainc, D. (2018). LRRK2 phosphorylation of auxilin mediates synaptic defects in dopaminergic neurons from patients with Parkinson's disease. *Proceedings of the National Academy of Sciences, 115*(21), 5576-5581.

Ratan, Y., Rajput, A., Pareek, A., Pareek, A., Jain, V., Sonia, S., . . . Singh, G. (2024). Advancements in genetic and biochemical insights: unraveling the etiopathogenesis of neurodegeneration in Parkinson's disease. *Biomolecules, 14*(1), 73.

Ravinther, A. I., Dewadas, H. D., Tong, S. R., Foo, C. N., Lin, Y.-E., Chien, C.-T., & Lim, Y. M. (2022). Molecular pathways involved in LRRK2-linked Parkinson's disease: a systematic review. *International journal of molecular sciences, 23*(19), 11744.

Frontier in Medical & Health Research

ISSN: (e) 3007-1607 (p) 3007-1593

Schwab, A. J., Sison, S. L., Meade, M. R., Broniowska, K. A., Corbett, J. A., & Ebert, A. D. (2017). Decreased sirtuin deacetylase activity in LRRK2 G2019S iPSC-derived dopaminergic neurons. *Stem cell reports, 9*(6), 1839-1852.

Senchuk, M. M., Van Raamsdonk, J. M., & Moore, D. J. (2021). Multiple genetic pathways regulating lifespan extension are neuroprotective in a G2019S LRRK2 nematode model of Parkinson's disease. *Neurobiology of disease, 151*, 105267.

Singh, A., Zhi, L., & Zhang, H. (2019). LRRK2 and mitochondria: recent advances and current views. *Brain research, 1702*, 96-104.

Tang, X., Xing, S., Ma, M., Xu, Z., Guan, Q., Chen, Y., . . . Chen, Y. (2023). The development and design strategy of leucine-rich repeat kinase 2 inhibitors: promising therapeutic agents for Parkinson's disease. *Journal of medicinal chemistry, 66*(4), 2282-2307.

Ullah, H., Ullah, A., Gul, H., Khan, R. U., Ahmad, J., Almeer, R., . . . Shah, Z. A. (2024). Interferon-stimulated gene (ISG12a) suppresses hepatitis B virus replication in Huh 7 cells line. *Journal of King Saud University-Science, 36*(9), 103377.

Xiong, Y., Dawson, T. M., & Dawson, V. L. (2017). Models of LRRK2-associated Parkinson's disease. *Leucine-Rich Repeat Kinase 2 (LRRK2)*, 163-191.

Xiong, Y., & Yu, J. (2024). LRRK2 in Parkinson's disease: upstream regulation and therapeutic targeting. *Trends in Molecular Medicine*.

Zhang, Z.-W., Tu, H., Jiang, M., Vanan, S., Chia, S. Y., Jang, S.-E., . . . Zhou, Z.-D. (2022). The APP intracellular domain promotes LRRK2 expression to enable feed-forward neurodegenerative mechanisms in Parkinson's disease. *Science Signaling, 15*(748), eabk3411.